Heikkinen, Ismo T.S.; Marin, Giovanni; Bihari, Nupur; Ekstrum, Craig; Mayville, Pierce J.; Fei, Yuhuan; Hu, Yun Hang; Karppinen, Maarit; Savin, Hele; Pearce, Joshua M.

# Atomic layer deposited aluminum oxide mitigates outgassing from fused filament fabrication–based 3-D printed components

*Published in:*
Surface and Coatings Technology

*DOI:*
10.1016/j.surfcoat.2020.125459

Published: 25/03/2020

*Document Version*
Peer-reviewed accepted author manuscript, also known as Final accepted manuscript or Post-print

*Please cite the original version:*
Heikkinen, I. T. S., Marin, G., Bihari, N., Ekstrum, C., Mayville, P. J., Fei, Y., Hu, Y. H., Karppinen, M., Savin, H., & Pearce, J. M. (2020). Atomic layer deposited aluminum oxide mitigates outgassing from fused filament fabrication–based 3-D printed components. *Surface and Coatings Technology*, *386*, Article 125459.
https://doi.org/10.1016/j.surfcoat.2020.125459

# Atomic layer deposited aluminium oxide mitigates outgassing from fused filament fabrication–based 3-D printed components

Ismo T.S. Heikkinen, Giovanni Marin, Nupur Bihari, Craig Ekstrum, Pierce J. Mayville, Yuhuan Fei, Yun Hang Hu, Maarit Karppinen, Hele Savin, Joshua M. Pearce

PII: S0257-8972(20)30128-6

DOI: https://doi.org/10.1016/j.surfcoat.2020.125459

Reference: SCT 125459

To appear in: *Surface & Coatings Technology*

Received date: 20 November 2019

Revised date: 30 January 2020

Accepted date: 8 February 2020

Please cite this article as: I.T.S. Heikkinen, G. Marin, N. Bihari, et al., Atomic layer deposited aluminium oxide mitigates outgassing from fused filament fabrication–based 3-D printed components, *Surface & Coatings Technology* (2018), https://doi.org/10.1016/j.surfcoat.2020.125459

# Atomic layer deposited aluminum oxide mitigates outgassing from fused filament fabrication–based 3-D printed components

Ismo T. S. Heikkinen[1§], Giovanni Marin[2§], Nupur Bihari[3§], Craig Ekstrum[3], Pierce J. Mayville[3], Yuhuan Fei[3], Yun Hang Hu[3], Maarit Karppinen[2], Hele Savin[1] and Joshua M. Pearce[1,3,4*]

1. Department of Electronics and Nanoengineering, School of Electrical Engineering, Aalto University, Espoo, Finland.
2. Department of Chemistry and Materials Science, School of Chemical Engineering, Aalto University, Espoo, Finland.
3. Department of Materials Science & Engineering, Michigan Technological University, Houghton, MI USA.
4. Department of Electrical & Computer Engineering, Michigan Technological University, Houghton, MI USA.

[§]These authors contributed equally to this publication.

* Electronic mail: pearce@mtu.edu

## Abstract

Open-source scientific hardware based on affordable fused filament fabrication (FFF) 3-D printing has the potential to reduce the cost of research tools considerably. So far, development has focused on tools that do not require compatibility with vacuum environments. Highly porous 3-D printed plastics require surface treatments to mitigate their outgassing, and in this study we explored the outgassing reduction from 3-D printed black-colored acrylonitrile butadiene styrene (ABS) and polycarbonate (PC) using a commercial vacuum sealing resin as well as atomic layer deposited (ALD) aluminium oxide ($AlO_x$). The outgassing properties of uncoated plastics could not be measured due to a too high level of outgassing, which was attributed to their high porosity and high specific surface area. However, both the commercial resin and the ALD coatings reduced the extent of outgassing from both ABS and PC, which enabled their comparison by residual gas analysis (RGA). Remarkably, the outgassing performance achieved with ALD $AlO_x$ was superior to the performance of the commercial vacuum resin across a temperature range of 40 to 100°C for both plastics, despite the uneven coverage of the plastic surface with $AlO_x$. Results indicated that both ABS and PC could be made compatible with at least moderate vacuums using ALD $AlO_x$. Thus, the fabrication of laboratory vacuum tools can be realized with affordable 3-D printed plastics. However, further studies on the physical mechanisms behind the outgassing reduction and the durability of the coatings are required.

**Keywords:** Atomic layer deposition, aluminium oxide, outgassing, vacuum compatibility, 3-D printed plastics

# I. INTRODUCTION

Additive manufacturing (AM) methods allow for rapid prototyping of designs and producing complex geometries that are not easily accessible by other manufacturing methods. In recent years, AM has facilitated the development of various open-source research tools, and especially affordable fused filament fabrication (FFF)–based 3-D printing shows great potential in laboratories in the fabrication of low-cost, customized, and high-quality scientific instruments [1-3]. Generally, these bespoke tools can reduce the cost of scientific equipment by 90-99% compared to commercial equipment, which has already created considerable value for the scientific community [4,5]. Examples of such tools include chemical mixers [6,7], microfluidic devices [8-11], and mass spectroscopy equipment [12], which highlights the various fields in which laboratories can benefit from open source scientific hardware.

Despite their promise, only a few short studies on using 3-D printed components in vacuum environments have been published [13-17]. Studies by Gans *et al.* [13] and Povilus *et al.* [14] mention that both the high porosity of FFF plastics and their lack of mechanical strength might pose issues in a vacuum. During the printing process, small voids and inclusions can form in the component, which can trap atmospheric gases. These gases can slowly leak into the vacuum environment, which increases the pressure in the vacuum vessel and renders the component incompatible with low-pressure applications. Other concerns in using plastics in vacuum environments are the high vapour pressure of the material itself, which can lead to significant amount of outgassing, and their limited thermal conductance. These issues have been discussed in previous studies [13, 15, 18, 19]. A potential approach to mitigate outgassing from 3-D printed plastics is to coat the component with metal layers [16] or by commercial vacuum sealing resins [17].

Atomic layer deposited (ALD) $AlO_x$ is a potential material for outgassing reduction, as layers that efficiently limit gas diffusion [20] can be deposited even at low temperatures [21-23] on various polymers [24]. ALD films have been demonstrated as viable layers for increasing the performance of polymers in space applications, such as protecting plastics from degradation [18] and potentially reducing outgassing of plastics at elevated temperatures [19]. In this study, we explore the mitigation of outgassing from affordable and easily printable FFF plastics using vacuum resins or thin inorganic aluminium oxide ($AlO_x$) coatings prepared by in house ALD. Specifically, we investigate the worst-case scenario using black pigmented plastics whose coloring agents can add to outgassing. The ultimate aim of these experiments is to create a toolkit for an open-source fully 3-D printable ALD tool, capable of producing high-quality ALD films for contamination-sensitive applications.

## II. EXPERIMENTAL

The investigated commercial 3-D printed materials were acrylonitrile butadiene styrene (ABS), which is one of the most common FFF plastics, and polycarbonate (PC), which is one of the highest strength plastics commonly available for standard FFF-based 3-D printers [25]. The plastics were coated with either a commercial vacuum sealing resin or ALD $AlO_x$, and the reduction of outgassing was compared using a residual gas analysis (RGA) tool. Black 3-D printed plastics were used to explore the limits of outgassing reduction, as a large number of concentrates used for black colouring are based on carbon black, which is a known outgassing agent [26]. The thermal and vacuum history of all samples were carefully matched to each other to provide an accurate analysis of the outgassing properties of the plastics.

## A. Sample preparation

3-D models of rectangular samples with the dimensions 5 mm × 5 mm × 2 mm and 30 mm × 30 mm × 1 mm were designed using OpenSCAD [27]. Uncoated 5 mm × 5 mm × 2 mm samples were used in surface area analysis, while the 30 mm × 30 mm × 1 mm were coated and used in outgassing studies. The samples were printed with an open source Lulzbot Taz 6 FFF-based 3-D printer (Aleph Objects, Loveland CO) using commercial 3-D printing filaments of ABS and PC. The ABS filament was obtained from IC3D (Ohio, USA), and PC (PC-Max) from Polymaker (Shanghai, China). The printer and slicing settings were determined with the Cura slicing software (21.08 Lulzbot edition), and the samples were printed with 100% infill using the printing parameters described in **Table 1**. PVA-based glue was applied to the printing bed before printing PC to decrease the adhesion between the samples and the printing bed. The residual glue was removed from the PC samples with particular care by wiping them with water-damped disposable laboratory wipes. After printing, both ABS and PC samples were handled with nitrile gloves and cleaned by consecutively wiping them with lint-free wipes damped in water and isopropanol.

TABLE 1. Essential printing parameters of the ABS and PC samples, defined using the Cura software.

| Plastic | Layer height [mm] | Shell thickness [mm] | Bottom/top thickness [mm] | Print speed [mm/s] | Top/bottom speed [mm/s] | Print *T* [°C] | Bed *T* [°C] | Minimal layer time [s] |
|---|---|---|---|---|---|---|---|---|
| ABS | 0.18 | 1.0 | 1.05 | 50 | 30 | 245 | 95 | 15 |
| PC | 0.15 | 1.0 | 0.9 | 50 | 30 | 255 | 100 | 20 |

The first sets of 30 mm × 30 mm × 1 mm ABS and PC samples were treated with a commercial silicone-based high vacuum leak sealing resin (Vacseal [28]), which was cured at 95°C for 24 hours [17]. The resin was applied to the top, bottom and sides of the samples using a brush. The second sample set of the same dimensions was coated with ALD $AlO_x$ using a Picosun R-100 top-flow ALD tool with trimethylaluminum (TMA) and deionized water as precursors. The reactor temperature was 80°C, which was below the glass transition temperature of both ABS (~105°C) and PC (~110°C) [29]. The reactor pressure was ~20 mTorr in a constant $N_2$ flow. TMA and water were dosed into the reactor from external containers kept at room temperature using pneumatic valves with pulse lengths 0.2 and 0.5 s, respectively, with 5 s purging steps between the precursor pulses. The samples were placed on top of silicon wafers used as monitor samples and coated with 300 cycles of $AlO_x$ per run in three consecutive runs, labelled depositions I, II, and III. Since the 3-D printed samples have high surface roughness there was some gas flow between the monitor wafer and the bottom of the plastic sample. The use of the monitor samples for film thickness characterization is further explained in the next section. Third sample set was made by applying the vacuum resin to the side facing the Si wafer during the deposition of some of the ALD-coated samples and curing them at 95°C at 24 hours. Uncoated samples were used as a reference set.

The vacuum histories of all samples were matched to the ALD-coated samples by placing the resin-coated and the reference samples in a vacuum chamber in ~20 mTorr pressure at 80°C for the duration of the ALD runs (~5 h). This sample pre-treatment was done to ensure that each sample had the opportunity to outgas and dehydrate before characterization. All sample sets and their corresponding coatings and pre-treatments are summarized in Table 2.

TABLE 2. Sample types and methods of pre-treatment. All samples were prepared for both ABS and PC.

| Sample set | ALD coating | Pre-treatment | Resin applied | Resin curing |
|---|---|---|---|---|
| Resin-coated | None | 80°C at 20 mTorr for 5 h | All sides | 95°C for 24 h |
| ALD-coated | 900 cycles $AlO_x$ at 80°C | None | No | None |
| Resin- and ALD-coated | 900 cycles $AlO_x$ at 80°C | None | Bottom side | 95°C for 24 h |
| Reference | None | 80°C at 20mTorr for 5 h | No | None |

## *B. Characterization*

The specific surface area of 3-D printed ABS and PC was determined using Brunauer-Emmett-Teller (BET) theory [30]. The nitrogen adsorption and desorption properties at liquid nitrogen temperature (77K) were investigated from one hundred pieces of the 5 mm × 5 mm × 2 mm samples using a Micromeritics ASAP 2000 instrument. PC and ABS samples were cryofractured and coated with conducting Pt:Pd in a 80:20 ratio, and scanning electron microscope (SEM) images were acquired with a Hitachi S-4700 field emission SEM (FE-SEM) to investigate the polymer cross-section microstructures. The same equipment was used for energy-dispersive X-ray spectroscopy (EDX) to identify the spatial distribution of elements in the micrographs. Depth profiling using X-ray photoelectron spectroscopy (XPS) was conducted using a PHI 5800 photoelectron spectrometer (Physical Electronics, Minnesota, USA) to check for carbon contamination in the deposited inorganic film.

A bespoke quadrupole residual gas analyser (RGA) setup, shown in Figure 1(a), was used in the outgassing experiments. The load lock region of a Riber molecular beam epitaxy system was connected to a roughing and turbo pump to create an isolated chamber capable of holding a vacuum of $10^{-7}$ Torr. A Transpector Inficon gas analysis system was installed on an available flange. A sample heater capable of reaching 100°C was mounted in the chamber and used to test the outgassing of the samples at 10°C increments, from base temperature (>36°C) until 100°C. Baseline partial pressure data using the RGA was gathered without a sample loaded at each temperature set point to characterize the inherent species present in an empty chamber. Samples were stored in a sealed desiccant container for a minimum of 24 hours prior to RGA analysis. Each sample was placed in the vacuum chamber at a base pressure of 1.7 to $2.3 \times 10^{-7}$ Torr for

12 hours before initiating the measurement. The partial pressures for species with 1 to 100 atomic mass units (AMU) were recorded using a TWare32 gas analysis software at the specified temperatures.

The data for each measurement was normalized using Eq. (1) to isolate the quantity of outgassed species:

$$PP = \frac{\left(\frac{PP_M}{P_0}\right)}{\left(\frac{PP_M^B}{P_0^B}\right)}, \qquad (1)$$

where

$PP_M$ is the partial pressure of the molecular mass of interest,
$P_0$ is the chamber pressure during the run,
$PP_M^B$ is the partial pressure of the molecular mass of interest during the baseline run (without sample),
$P_0^B$ is the chamber pressure during the baseline run.

Due to the variation in base pressure during each run, the partial pressure in both the numerator and the denominator were divided by the base pressure during that run. The noise level of the partial pressure measurement was approximately $10^{-15}$ Torr, so data below this limit was discarded.

During the ALD depositions, 4-inch silicon wafers (Okmetic, n-type, 300 µm, 2-5 Ω/cm, double-side polished, 100 orientation) were used as monitor samples to facilitate the characterization of film growth in the ALD runs. Initially, a 30 mm × 30 mm piece of a similar Si wafer was placed on top of a monitor wafer to study how the geometry of the samples affect the film growth. A schematic explaining the sample positioning inside the ALD reactor is presented in Figure 1(b). One 3-D printed plastic sample at a time was placed on a monitor wafer, and the samples were coated with 300 cycles of $AlO_x$ per run in three consecutive runs (runs I-III). The monitor wafer was changed for each individual run to observe if the increasing film thickness on the plastic sample would influence the outgassing in such a degree that changes could be seen in the properties of the ALD film. Therefore, the plastic samples had 900 cycles of $AlO_x$ on them after all the runs, while all monitor samples had only 300 cycles on them. The difference between each monitor sample was that the thickness of the $AlO_x$ on the plastic sample placed on top of the wafer was different.

ALD film thickness and density were determined from the monitor samples using X-ray reflectometry (XRR) (PANalytical X`Pert) in four areas per wafer to study how the potential outgassing from the plastic pieces would influence the growth rate and density of the $AlO_x$ film on silicon. This provides indirect information on the amount of outgassing from the plastics, as volatile compounds potentially perturb the precursor flow over the samples. The thickness map was created with an ellipsometer (J.A. Woollam M2000UI) scan of full wafer area giving better thickness data compared to the XRR analysis. Additionally, a J.A. Woollam V-VASE spectroscopic ellipsometer was used at angles 65°, 70° and 75° (wavelength = 300 to 900nm in steps of 10nm) to determine refractive index at certain selected points which were shown to have similar thickness.

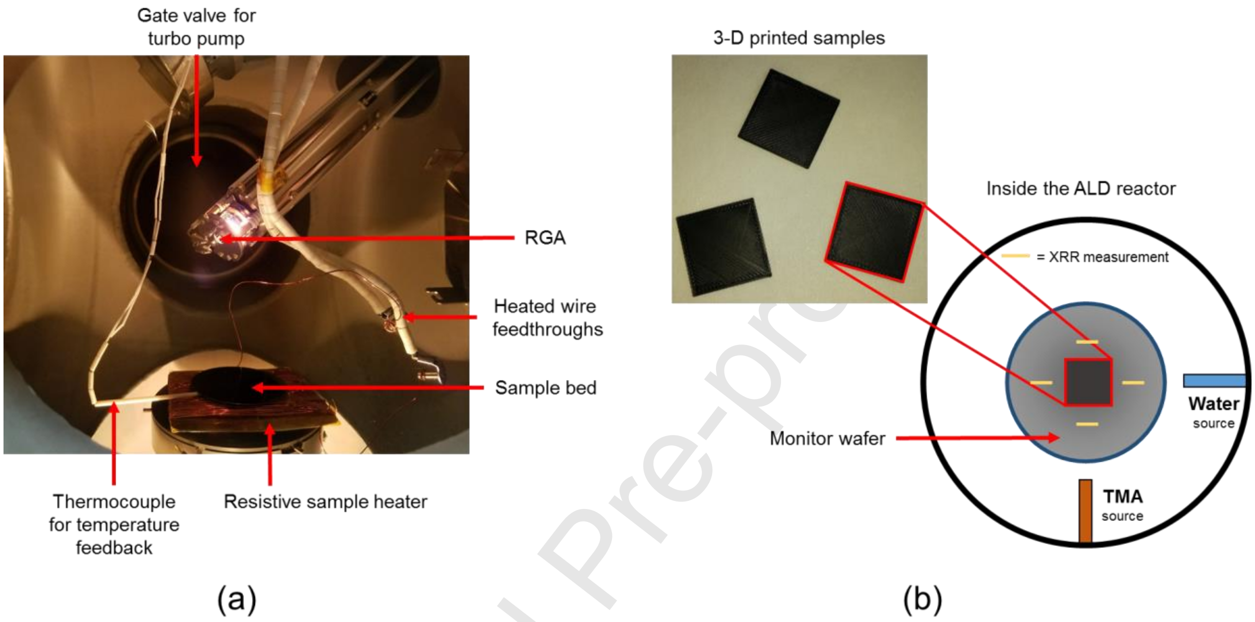

FIG 1. (a) Modified load lock of MBE system showing sample heater, polymer sample and RGA. (b) 3-D printed 30 mm × 30 mm × 1 mm plastic samples were placed on a silicon wafer inside the ALD chamber. The yellow lines mark the locations where the ALD AlOx film thickness and density were measured with XRR. The thickness of the AlOx film was also mapped across the whole monitor wafer with ellipsometry.

## III. RESULTS

Thickness measurements on the monitor Si wafers confirmed that the presence of both ABS and PC made the $AlO_x$ film grow non-uniformly. In the reference deposition, in which the 30 mm × 30 mm silicon piece was on top of the monitor wafer, the film thickness ranged from 39 nm (further away from the precursor inlets) to 46 nm (directly after the inlets). During the initial depositions on ABS and PC samples, a more severe disruption of the film growth on the monitor wafers compared to the square silicon sample was observed. Pictures of the wafers and the respective thickness maps are shown in Figure 2, and it was observed that the $AlO_x$ film did not grow uniformly on the surface of the monitor wafer. There was higher growth in the area near the TMA inlet and lower on its opposite side. Around the edges of the plastic samples, highly irregular growth that was limited around and below the samples was observed. With each consequent step of the deposition, the uniformity of the film on the monitor wafer improved slightly, which suggested changes in the outgassing, the surface properties of the plastic, or introduction of new alumina nucleation sites that contribute to the outgassing barrier properties. XRR measurements on the monitor samples revealed that film density remained essentially constant (values) among the four measurement areas for both ABS and PC in all monitor wafers.

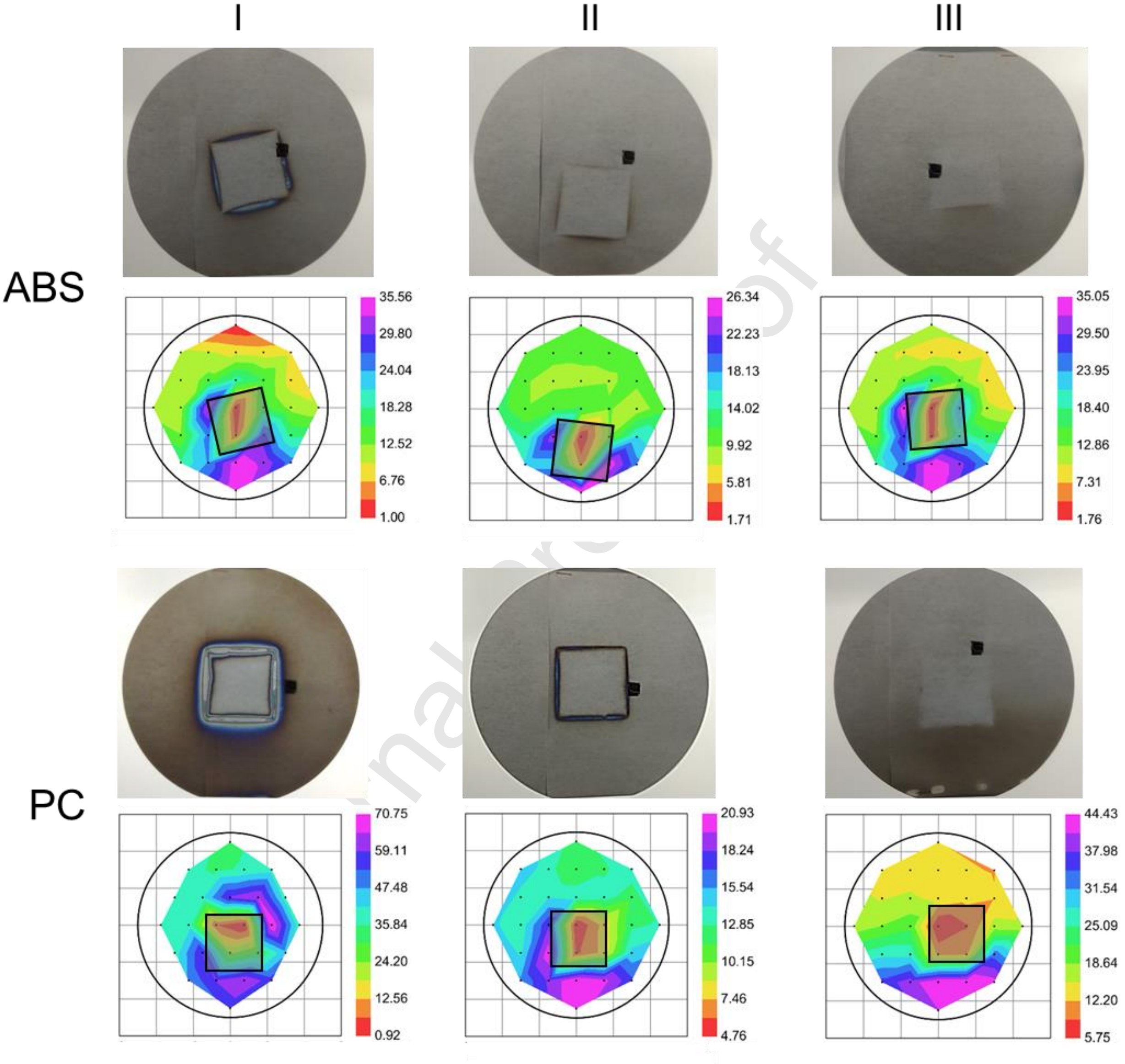

FIGURE 2. Photographs and ellipsometry maps of the monitor wafer after each sequential (I-III) ALD run for ABS and PC. The thickness maps close to the plastic sample position are not accurate because of uncontrolled film deposition. The non-uniformity of the deposition is clear in both photos and ellipsometer maps. The thickness scale [nm] is on the right of each map.

Characterization of the 3-D printed plastics revealed that both materials were highly porous. Based on the BET analysis, the specific surface area of uncoated ABS was 0.91 $m^2/g$, while for PC it was 1.08 $m^2/g$. SEM images of the cryofractured ABS and PC cross sections are shown in Figure 3. The average pore diameter in PC was approximately 500 nm, while the pore size distribution in ABS was much larger, ranging from the nanometer to the micrometer range.

Based on the SEM images, it was estimated that the pores accounted for approximately 28% of the volume of the ABS sample, while for PC ~56% of the volume comprised of pores. When uncoated ABS and PC samples were loaded into the testing chamber and pumped down, the base pressure of the system did not get down to a level low enough for the RGA to function. Therefore, the need for reduction of outgassing from both ABS and PC was evident in order to use them in vacuum applications.

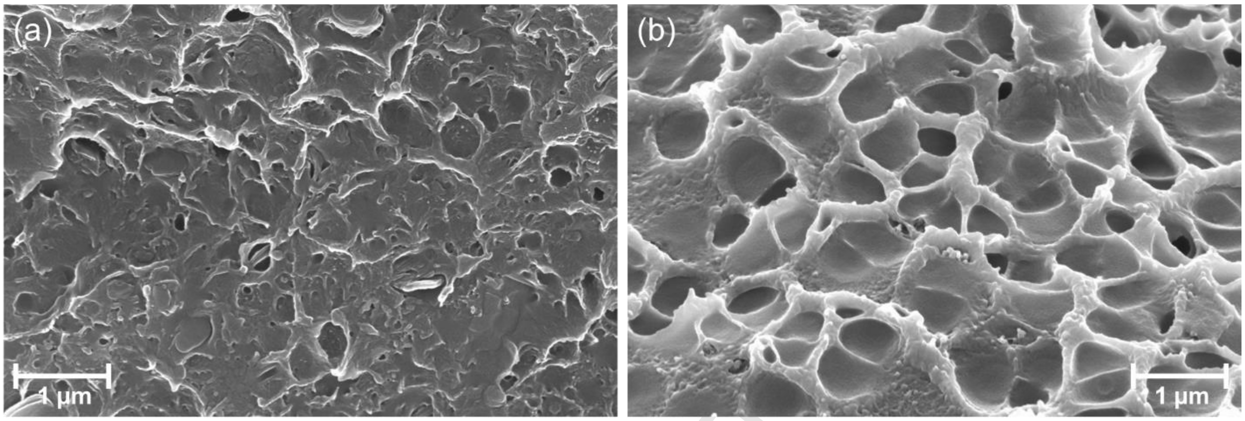

FIGURE 3. SEM micrographs of cryo-fractured cross-sections of uncoated 3-D printed (a) ABS and (b) PC, showing porous structures.

Coating the plastics with an approximately 7 µm thick layer of the commercial vacuum resin smoothened the surfaces substantially, as seen for the resin-coated PC sample in Figure 4(a). The resin had partially penetrated the porous surface, and the pore size seemed to increase towards the bulk of the sample. SEM images of the PC surface show both surface cracks and point defects on the resin layer (Figure 4(b) and 4(c)), which indicated that the application of the resin and the curing process were not optimal to achieve perfect surface coverage.

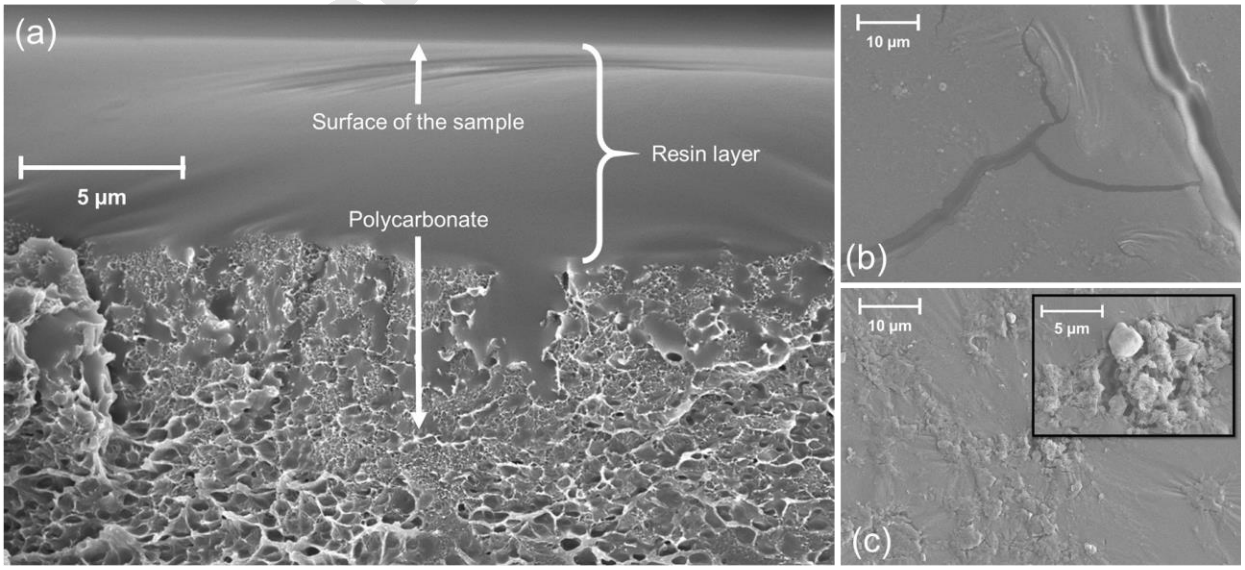

FIGURE. 4.(a) Cryo-fractured cross-section of 3-D printed PC sample, coated with the commercial vacuum resin. The image shows partial penetration of the resin into the pores of the plastic. Pore size was smaller close the surface of the sample than in the bulk. (b) PC surface showing cracks in the vacuum resin. (c) Accumulation of resin on the PC surface with the inset showing a magnified view of resin clusters.

SEM images and EDS analysis of the ALD-coated plastics revealed that the $AlO_x$ coating was fully conformal on the surface of PC, whereas the surface of ABS exhibited regions devoid of an oxide coating (Figure 5). ALD layers on both polymers were found to include 3-D growth, with clusters of $AlO_x$ appearing to grow vertically from the film surfaces (Figures 5 and 6). EDS confirmed the composition of the observed particulates to be a majority of Al and O, suggesting that they were monocrystals or polycrystals of $AlO_x$. The particles had a diameter of 1-2 µm. The presence of particulates suggests that the layer-by-layer reaction sequence characteristic to ALD growth was interrupted. It is possible that TMA and water molecules desorbed from the polymers reacted with each other in the gas phase, subsequently precipitating, or free water vapor pre-emptively reacted with TMA adsorbed to the polymer surface during the precursor stage of the ALD cycle.

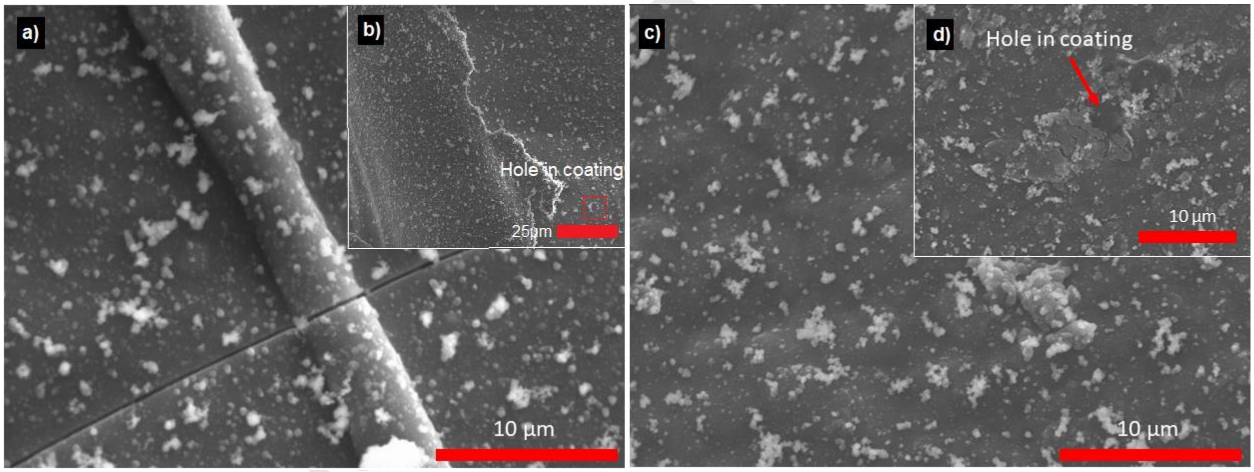

FIGURE 5. SEM image of (a) PC ALD coating (BSE image), (b) inset image of hole in PC ALD coating, (c) ABS ALD coating (BSE image), (d) inset image of hole in ABS ALD coating.

The presence of fracture in the ALD layer on the PC samples is telling of the layer's uniform mechanical properties and contiguousness. No fractures were noted in the ALD on the ABS sample's surface, which further exemplifies the non-contiguous nature of the film as shown in Figure 5, having sizeable gaps in the film.

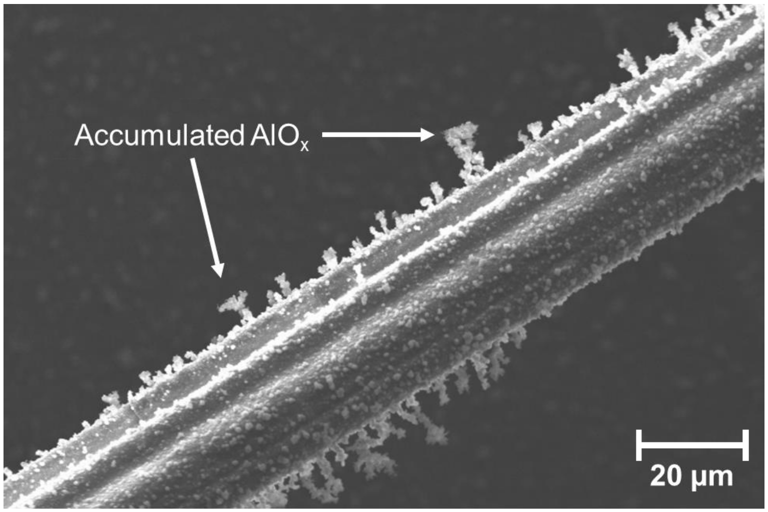

FIGURE 6. SEM image of a strand of PC, coated with 900 cycles of $AlO_x$. Instead of growing as a uniform film, the $AlO_x$ had accumulated on the plastic surface as micron-sized particles and whiskers.

Subsurface crystallites of $AlO_x$ were observed in both polymers, contained mostly within a depth of 5 µm relative to the ALD coating/polymer interface. Due to the small size of the pores in each polymer, it was difficult to determine if a direct association between subsurface crystallites and pores existed, but the size of the crystallites in the PC sample seems to corroborate this possibility.

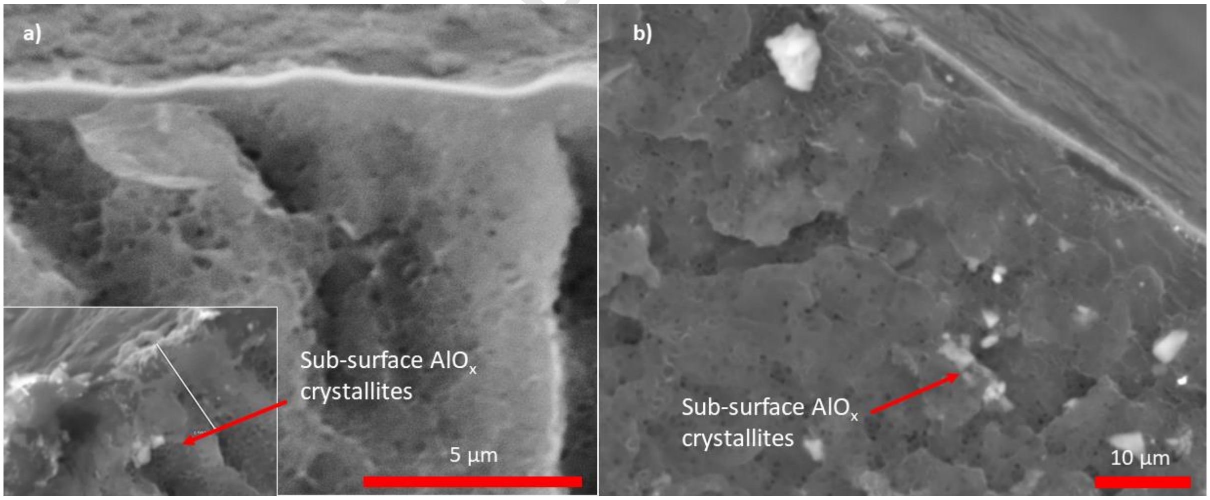

FIGURE 7. Backscattered SEM cross section images of (a) black ABS with ALD coating and (b) black PC ALD coating. Note the presence of sub-surface $AlO_x$ crystallites, identified via EDS. An example EDS line scan path is presented in the sub-set image for the black ABS image.

Both ALD-coated polymers showed sub-surface agglomerates of $AlO_x$, with similar penetration depth of Al and O, as determined from EDS line scans (Figure 8). Line scans locations were chosen to avoid subsurface crystallites, in order to sample the bulk subsurface composition. The presence of subsurface Al Kα and enhanced O Kα signal is assumed to result from the presence of subsurface $AlO_x$ crystallites, dispersed finely in the matrix (distinct from the agglomerates shown in Figure 7). The higher O Kα signal in the PC sample relative to the ABS sample at increasing depths from the coating surface reflects the presence of O in the structure of the polymer. Another notable difference between the EDS line scans is the continual increase in C Kα signal with depth from the ALD layer, as we go deeper into the sample.

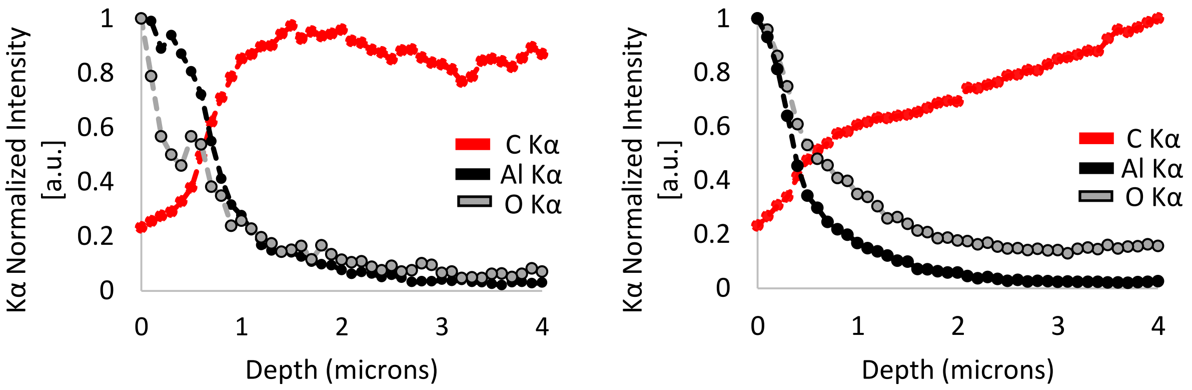

Figure 8. Depth profiles of C, O, and Al Kα signal from EDS line scan (left: black ABS, right: black PC). Depth measured as linear distance from the maximum Al Kα signal position (assumed to be the centreline of the $AlO_x$ coating). Line scans were taken with an accelerating voltage of 15 kV and each elemental Kα profile is normalized to the maximum intensity within the sampling length.

After coating the samples and the preparation procedures, the outgassing from all samples was analysed with the RGA setup. For resin- and ALD-coated ABS and both resin-containing PC samples, the summed partial pressure of all outgassing species increased with temperature. This led to a substantial increase in total chamber pressure, and a very high filament current was registered at temperatures over 80 °C for resin-coated ABS, over 50°C for resin- and ALD-coated PC and over 60°C for resin-coated PC. In order to protect the RGA from damage, data collection from these samples was terminated at the aforementioned temperatures.

The sum of the normalized partial pressures from 1 to 100 AMU for each temperature are presented in Figure 7a) for ABS and b) for PC. For both plastics, the outgassing level of the ALD-coated remained the lowest at all temperatures. The outgassing from the resin-coated ABS was the highest of all ABS samples until 60°C, after which the resin- and ALD-coated sample showed a sudden increase in outgassing. Above 70°C, the outgassing from resin-coated ABS started to decrease, but the outgassing level was still higher at 100°C than that of the ALD-coated samples. Similar to ABS, the resin-coated PC samples showed the highest outgassing level, and the outgassing from the resin- and ALD-coated samples was between the level of resin-coated and ALD-coated samples. At certain temperatures the resin- and ALD-coated samples exhibited outgassing higher than resin-coated samples. Since the coating was applied to the backside manually and great care was taken to ensure it does not overlap the ALD coating on the front, parts of it may have been accidentally applied too thick, leading to higher outgassing seen at elevated temperatures.

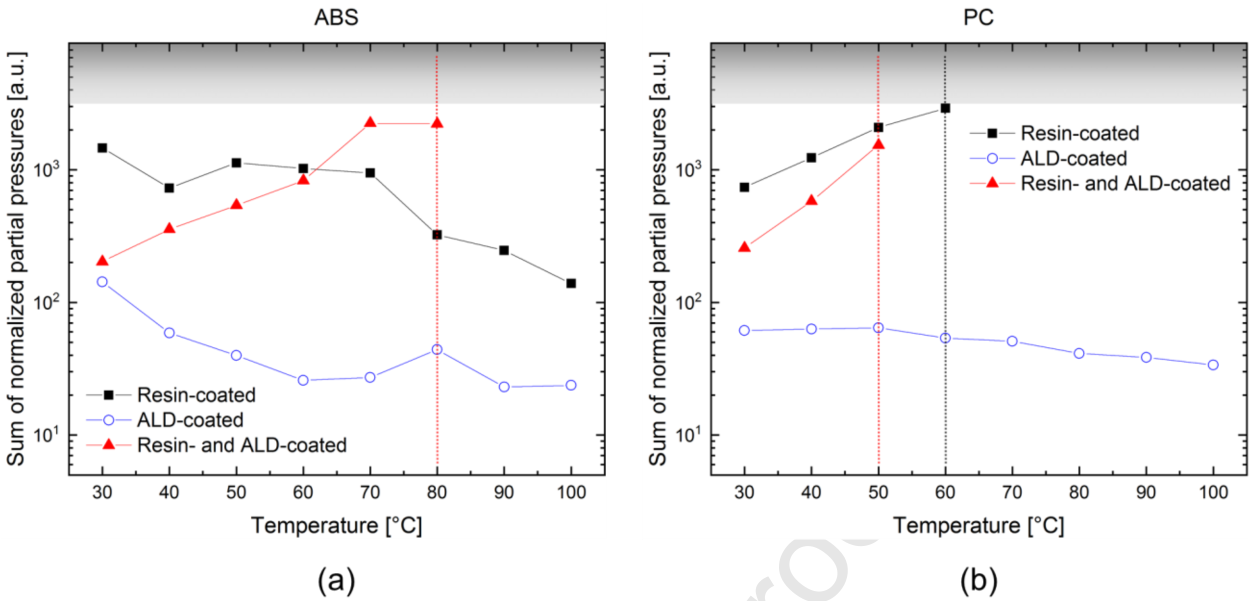

FIGURE 9. Sum of the normalized partial pressures for each temperature for (a) ABS and (b) PC. Due to a high amount of outgassing from samples with the resin, the outgassing could not be measured at all temperatures with limits indicated with dashed lines. Estimate for the pressure that was too high for the RGA measurement is indicated in the graphs as the grey area. The outgassing from the ALD-coated samples remained low throughout the studied temperature range. The acceptable partial pressure value is determined by the end user's application.

Comparison of the outgassing properties of all samples was done at 50°C to highlight the influence of the coatings. Figure 8 presents the normalized partial pressure of outgassing species with molecular mass ranging from 1 to 100 AMU at 50°C from all sample sets. The partial pressures of the outgassing species from the resin-coated samples were lower than from uncoated reference samples, but compared the other coatings the resin-coated samples had the highest amount of outgassing. Resin- and ALD-coated samples registered intermediate outgassing pressures. This was especially evident at molecular masses >50 AMU. The overall outgassing level of ALD-coated samples was noticeably and consistently lower than from the samples that had resin on them.

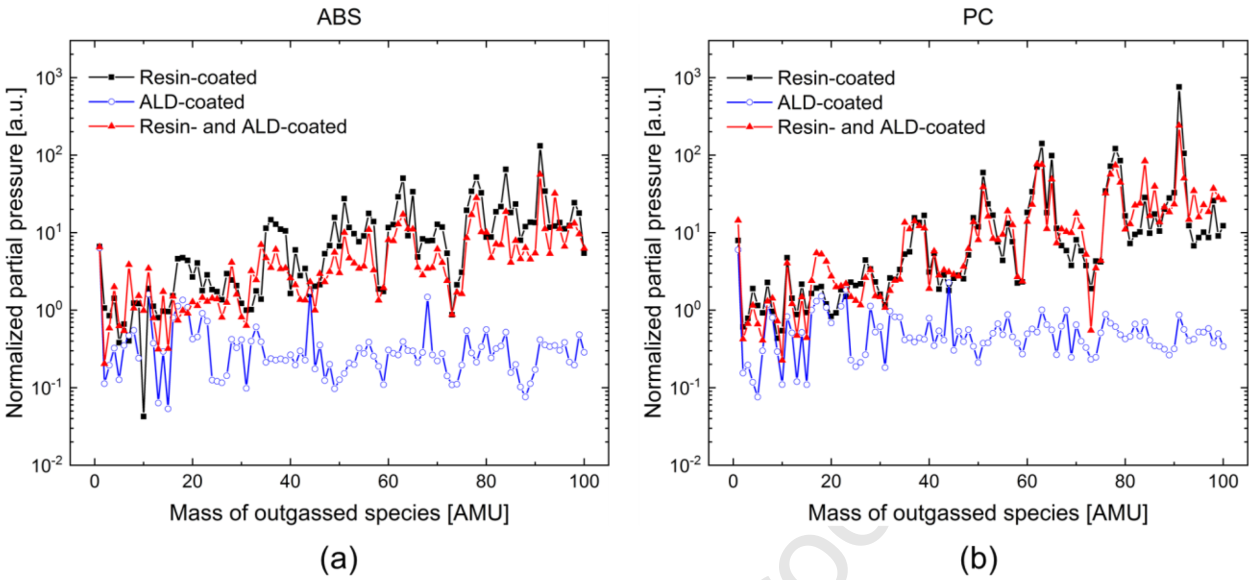

FIG. 10. A comparison of outgassing characteristics of coated ABS (a) and PC (b) samples at molecular masses 1 to 100 AMU at 50 °C, showing a consistently low value for the ALD-coated samples.

# IV. DISCUSSION

3-D printed polymers are known to have high porosity due to voids present in the microstructure [31-33]. While the presence of these voids can be exploited to tune mechanical properties for various biological applications [34], the high porosity and specific surface area of both 3-D printed ABS and PC posed a challenge for their use in vacuum applications, as the uncoated polymers had such a high level of outgassing that the RGA measurements could not be conducted. The pores in the material had the potential to trap atmospheric contaminants that likely escaped in the presence of vacuum. Coating the 3-D printed plastics with either a commercial vacuum sealing resin or ALD $AlO_x$ reduced the outgassing to a level that was measurable with the employed setup. Resin-coated ABS exhibited a lower total amount of outgassing compared to PC. The higher porosity and higher specific surface area of PC potentially contributed to higher adsorption of ambient gases, resulting in serious outgassing of atmospheric contaminants under vacuum. The resin did not provide a uniform and durable coverage of the plastic surfaces, seen as cracks on the PC surface. This effect was seen to a comparatively lower extent in ABS due to its lower porosity.

A potential explanation for the decrease of pore size at the surface is the curing procedure, as at 95°C the plastics could have softened even below the glass transition temperature. SEM micrographs of the surfaces coated with the vacuum resin showed cracking, which appeared when the solvent was driven off using a baking process at elevated temperature to cure the resin. This cracking was attributed to the possible large thickness of the resin, due to which it could not be cured effectively. Hence, when the solvents were drawn out, the polymer potentially contracted and clusters of the resin could be seen on the surface. This problem may be mitigated by gradually heating the sample to eliminate the possibility of thermal shock.

Based on the deposition on a 30 mm × 30 mm Si sample on top of a monitor wafer, it was concluded that the physical presence of the sample in the middle of the deposition area influenced the film uniformity. Based on previous studies, even minor changes to the sample placement inside the reactor can affect the gas flow on top of the wafer [35]. In the course of the $AlO_x$ depositions, it was observed that the plastics disrupted the growth of the film. The species that outgassed from the plastics were likely parts of both ABS and PC polymer chains. These hydrocarbons speculatively adsorbed to the substrate surface of the monitor Si wafer during deposition, preventing TMA molecules from reaching the active surface OH-sites. This reduced the film thickness across the wafer. On all the four sides of the chamber, there were inlets with a constant flow of $N_2$ carrier gas that moved the outgassed products all over the chamber, disrupting the deposition more the further from the precursor inlet. A higher growth area did not appear in front of the water inlet suggesting that the water reaches further away from the inlet compared to TMA. On the other hand, uncontrollably rapid growth was observed in the initial deposition in areas that were in contact with the plastics. A likely explanation for this is the adsorption of water during the water pulse into the porous structure of the plastic, and its subsequent release during the TMA pulsing steps. TMA molecules reacted with the higher excess water molecules around the plastic in the gas phase. The gradual release of water led to high film thickness localized to the edges of the plastics and reducing the film uniformity. The presence of water vapor during the TMA pulse also explains the formation of the $AlO_x$ clusters that were deposited on the surface of the plastics. As these particulates can be difficult to remove from vacuum systems, their formation should be suppressed by lengthening the purge step in the ALD process when coating porous substrates.

Despite the non-optimal ALD process, the uniformity of the film that was deposited on the monitor wafer improved with increasing $AlO_x$ thickness on the plastic. This can be attributed to the reduction of outgassing and lower amount of water adsorption to the surface of the plastic, which was seen as reduced amount of uncontrolled growth around the edges of the sample. The physical presence of the plastic likely played a role in decreasing the uniformity of the film away from the precursor's inlets, but its effect was difficult to detect in these depositions, since the outgassing and water absorption likely had a larger influence on the film uniformity in the initial depositions. However, in run III, the disruption of precursor flows due to the physical shape of the sample might have started to influence the film uniformity.

The outgassing characteristics were the least favourable for the resin-coated samples. However, it should be noted that the resin did reduce the outgassing enough for both materials to be measured by the RGA. Intermediate outgassing characteristics were observed for the ALD-coated samples that also had vacuum resin on them. It was speculated that although the resin is meant for vacuum applications, its incomplete curing can cause continued outgassing. The resin manufacturer [36] states that the recommended curing temperature of this product is 200°C, and room temperature curing, while possible, is not recommended. Since the plastics would melt at such a high temperature, curing was done at 95°C, which was below the glass transition temperature of both plastics. This may have been insufficient for this purpose, as the amount of outgassing continued to decrease from resin-coated ABS at temperatures above 70°C. In addition, as the resin was applied to the plastic samples using the brush provided by the manufacturer, it is probable that a too thick layer was deposited, leading to insufficient curing.

The solvents in the vacuum resin potentially continued to outgas during the RGA tests. While the precise composition of the sealant was not available, the concentration of xylene was the highest in the proprietary mixture [37], other constituents being ethylbenzene and toluene. As a preliminary test, the known mass spectrums of p-xylene, ethylbenzene and toluene [38] were compared to the partial pressure data obtained from resin-coated ABS and PC samples. The highest peak at molecular mass 91 AMU was matched to all three of these compounds. In addition, a minor peak at 67 AMU was also matched to xylene. This indicated the need to sufficiently cure the sealant to drive off solvents before use in a vacuum environment. With the curing protocol used in this study, the commercial vacuum cleaning resin is not recommended as a coating to prevent outgassing of FFF-based 3-D printed vacuum components. Instead, substantial outgassing reduction from 3-D printed plastics could be obtained with ALD $AlO_x$, even with a non-optimal growth process.

The collected outgassing data indicated that ABS had better overall outgassing characteristics than PC, as the resin-coated ABS samples had consistently lower normalized partial pressure values for outgassed species with molecular masses in the range of 1-100 AMU than PC. One of the NASA standard metrics to quantify outgassing is water vapour regained (WVR) [39]. 3-D printed ABS has a higher WVR value (0.25%) compared to PC (0.14%) [40]. In fact, it has been reported that at least 80% out of all gas absorbed in ABS is water vapour [41] and that most water vapour selectively outgasses in the mTorr pressure range [42-43]. In this study, all outgassing data was collected below 1 mTorr, indicating that ABS had dehydrated more effectively. The presence of other gases in PC, such as $CO_2$, CO and $H_2$ [44], and their slow removal rates may have contributed to its undesirable outgassing characteristics. However, the ALD $AlO_x$ coating significantly reduced the amount of outgassing from both materials, enabling the use of plastics with beneficial thermal tolerance but poor outgassing properties in vacuum systems operating in the mTorr range.

While the coatings may serve as adequate barriers against outgassing, any defects in the coating will allow volatile organic compounds as well as particulate carbon black to escape and potentially contaminate the vacuum system. Hence, more detailed characterization of the outgassed species of ALD-coated FFF plastics is required to ensure that the plastic parts used in a vacuum chamber would not contaminate the system. Uncoloured 3-D printed plastics would be preferable materials for vacuum components.

The reason why the ALD-coated samples remarkably exhibited the lowest level of outgassing can potentially be attributed to the reduction of surface area and water adsorption capability by the $AlO_x$ clusters seen in the SEM images. However, the exact mechanism for outgassing reduction by ALD $AlO_x$ was not unveiled in these studies, and this issued is to be addressed in further studies. The density of the ALD $AlO_x$ films was constant from run to run with or without the plastic inside the reactor. This was an indirect indication that the outgassed species were not incorporating into the film during the growth. XPS measurements on the $AlO_x$ films showed that carbon had only incorporated into the top ~5 nm of the film, which was attributed to atmospheric contamination present in all samples. This, in turn confirmed that the outgassed hydrocarbons from the plastics did not react chemically with the precursors used in this process. This was verified by measuring the refractive index at certain spots with similar thickness. In areas with thickness ≈20nm, the refractive index was found to be ≈3 at 600nm.

The printing parameters for these materials may be altered to reduce the porosity of the printed components. Some degree of over-extrusion coupled with heat treatments could provide a smoother surface, which would be less prone to outgassing and vapour absorption. Apart from ALD coated ABS and PC that have potential for use in vacuum environments [40], ALD coated polypropylene (PP) may also be utilized in 3-D printed vacuum processing tools because of its chemical inertness [29], cleanroom compatibility [45] and higher crystallinity [46].

More work is required to confirm the physical mechanisms behind the reduction of outgassing, and in future experiments focusing on this, a PID controlled heater could be used in the vacuum system to keep the ramp rate consistent across all the ten-degree increments. In addition, a spacer could be used to elevate the sample during outgassing tests so that the distance between the sample and the RGA is reduced. Further studies are also needed to determine the long-term stability of the outgassing reduction using ALD coatings, as the underlying 3-D printed plastic and $AlO_x$ have different thermal expansion coefficients. Repeated thermal cycling from low to high temperature can lead to fracturing of the ALD film and impair the outgassing properties of the plastic.

## V. CONCLUSIONS

The reduction of outgassing from affordable FFF-based 3-D printed ABS and PC using a commercial vacuum sealing resin and an inorganic ALD $AlO_x$ coating was demonstrated, providing a basis for using commercial 3-D printed plastics in vacuum applications. Resin-coated ABS had better outgassing properties than resin-coated PC, which was attributed to the lower porosity and specific surface area of ABS compared to PC. However, an ALD $AlO_x$ coating with thickness in the order of hundreds of nanometres was shown to significantly reduce the outgassing from both ABS and PC. The 3-D printed plastics disturbed the growth of the ALD film potentially due to outgassing and precursor adsorption into the sample surface, but their influence gradually reduced with increasing ALD coating thickness. Outgassing analysis showed that inorganic ALD $AlO_x$ coatings effectively reduced outgassing from both ABS and PC, even with uneven and non-conformal coverage of the plastics. The vacuum sealing resin was not as effective as the ALD coatings in reducing the outgassing, likely because a non-optimal curing process had to be used due to the limited thermal resilience of the 3-D printed plastics. The results presented in this study provide a clear basis for using affordable FFF-based plastic components in vacuum chambers.

# ACKNOWLEDGMENTS

This work was partially supported by Fulbright Finland, the Witte endowment and Aleph Objects. The authors acknowledge the provision of facilities by Aalto University at OtaNano – Micronova Nanofabrication Centre and at the RawMatTERS (RAMI) facilities, and the Applied Chemical and Morphological Analysis Laboratory at Michigan Tech for use of the instruments and staff assistance. Parts of this study were completed using Michigan Technological University's Microfabrication Facility. I.T.S.H. acknowledges the financial support from Aalto ELEC Doctoral School and Walter Ahlström foundation. G.M. and M.K. gratefully acknowledge funding from the Strategic Research Council at the Academy of Finland (CloseLoop Consortium, Grant No. 303452).

## REFERENCES

[1] Pearce, J. (2012). Building Research Equipment with Free, Open-Source Hardware. Science, 337(6100), pp.1303-1304. doi.org/10.1126/science.1228183

[2] Pearce, J.M., 2013. *Open-source lab: how to build your own hardware and reduce research costs*. Newnes.

[3] Pearce, J.M., 2014. Laboratory equipment: Cut costs with open-source hardware. *Nature*, *505*(7485), p.618. doi.org/10.1038/505618d

[4] Pearce, J.M., 2015. Return on investment for open source scientific hardware development. *Science and Public Policy*, *43*(2), pp.192-195. doi.org/10.1093/scipol/scv034

[5] Baden, T., Chagas, A.M., Gage, G., Marzullo, T., Prieto-Godino, L.L. and Euler, T., 2015. Open Labware: 3-D printing your own lab equipment. *PLoS biology*, *13*(3), p.e1002086. doi.org/10.1371/journal.pbio.1002086

[6] Dhankani, K.C. and Pearce, J.M., 2017. Open source laboratory sample rotator mixer and shaker. *HardwareX*, *1*, pp.1-12. doi.org/10.1016/j.ohx.2016.07.001

[7] Trivedi, D. and Pearce, J., 2017. Open source 3-D printed nutating mixer. *Applied Sciences*, *7*(9), p.942. doi.org/10.3390/app7090942

[8] da Costa, E.T., Mora, M.F., Willis, P.A., do Lago, C.L., Jiao, H. and Garcia, C.D., 2014. Getting started with open- hardware: Development and control of microfluidic devices. *Electrophoresis*, *35*(16), pp.2370-2377. doi.org/10.1002/elps.201400128

[9] Bhattacharjee, N., Urrios, A., Kang, S. and Folch, A., 2016. The upcoming 3D-printing revolution in microfluidics. *Lab on a Chip*, *16*(10), pp.1720-1742. doi.org/10.1039/C6LC00163G

[10] Morgan, A.J., San Jose, L.H., Jamieson, W.D., Wymant, J.M., Song, B., Stephens, P., Barrow, D.A. and Castell, O.K., 2016. Simple and versatile 3D printed microfluidics using fused filament fabrication. *PloS one*, *11*(4), p.e0152023. doi.org/10.1371/journal.pone.0152023

[11] Pearce, J.M., Anzalone, N.C. and Heldt, C.L., 2016. Open-source wax RepRap 3-D printer for rapid prototyping paper-based microfluidics. *Journal of laboratory automation*, *21*(4), pp.510-516. doi.org/10.1177/2211068215624408

[12] Maldonado-Torres, M., López-Hernández, J.F., Jiménez-Sandoval, P. and Winkler, R., 2014. 'Plug and Play'assembly of a low-temperature plasma ionization mass spectrometry imaging (LTP-MSI) system. *Journal of proteomics*, *102*, pp.60-65. doi.org/10.1016/j.jprot.2014.03.003

[13] Gans, A.R., Jobbins, M.M., Lee, D.Y. and Alex Kandel, S., 2014. Vacuum compatibility of silver and titanium parts made using three-dimensional printing. *Journal of Vacuum Science & Technology A: Vacuum, Surfaces, and Films*, *32*(2), p.023201. doi.org/10.1116/1.4846195

[14] Povilus, A.P., Wurden, C.J., Vendeiro, Z., Baquero-Ruiz, M. and Fajans, J., 2014. Vacuum compatibility of 3D-printed materials. *Journal of Vacuum Science & Technology A: Vacuum, Surfaces, and Films*, *32*(3), p.033001. doi.org/10.1116/1.4873556

[15] Zwicker, A.P., Bloom, J., Albertson, R. and Gershman, S., 2015. The suitability of 3D printed plastic parts for laboratory use. *American Journal of Physics*, *83*(3), pp.281-285. doi.org/10.1119/1.4900746

[16] Rivera, W.F. and Romero-Talamás, C.A., 2016. Vacuum compatibility of 3-d-printed parts. *IEEE Transactions on Plasma Science*, *44*(5), pp.874-876. doi.org/10.1109/TPS.2016.2540924

[17] Chaneliere, T., 2017. Vacuum compatibility of ABS plastics 3D-printed objects. CNRS, Laboratoire Aimé Cotton.

[18] Minton, T.K., Wu, B., Zhang, J., Lindholm, N.F., Abdulagatov, A.I., O'Patchen, J., George, S.M. and Groner, M.D., 2010. Protecting polymers in space with atomic layer deposition coatings. *ACS applied materials & interfaces*, *2*(9), pp.2515-2520. doi.org/10.1021/am100217m

[19] Kestilä, A., Nordling, K., Miikkulainen, V., Kaipio, M., Tikka, T., Salmi, M., Auer, A., Leskelä, M. and Ritala, M., 2018. Towards space-grade 3D-printed, ALD-coated small satellite propulsion components for fluidics. *Additive Manufacturing*, *22*, pp.31-37. doi.org/10.1016/j.addma.2018.04.023

[20] Groner, M.D., George, S.M., McLean, R.S. and Carcia, P.F., 2006. Gas diffusion barriers on polymers using Al 2 O 3 atomic layer deposition. *Applied Physics Letters*, *88*(5), p.051907. doi.org/10.1063/1.2168489

[21] Ferguson, J.D., Weimer, A.W. and George, S.M., 2004. Atomic layer deposition of Al2O3 films on polyethylene particles. *Chemistry of materials*, *16*(26), pp.5602-5609. doi.org/10.1021/cm040008y

[22] Wilson, C.A., Grubbs, R.K. and George, S.M., 2005. Nucleation and growth during Al2O3 atomic layer deposition on polymers. *Chemistry of Materials*, *17*(23), pp.5625-5634. doi.org/10.1021/cm050704d

[23] Hirvikorpi, T., Vähä-Nissi, M., Mustonen, T., Iiskola, E. and Karppinen, M., 2010. Atomic layer deposited aluminum oxide barrier coatings for packaging materials. *Thin Solid Films*, *518*(10), pp.2654-2658. doi.org/10.1016/j.tsf.2009.08.025

[24] Parsons, G.N., Atanasov, S.E., Dandley, E.C., Devine, C.K., Gong, B., Jur, J.S., Lee, K., Oldham, C.J., Peng, Q., Spagnola, J.C. and Williams, P.S., 2013. Mechanisms and reactions during atomic layer deposition on polymers. *Coordination Chemistry Reviews*, *257*(23-24), pp.3323-3331. doi.org/10.1016/j.ccr.2013.07.001

[25] Tanikella, N.G., Wittbrodt, B. and Pearce, J.M., 2017. Tensile strength of commercial polymer materials for fused filament fabrication 3D printing. *Additive Manufacturing*, *15*, pp.40-47. doi.org/10.1016/j.addma.2017.03.005

[26] Puri, B.R. and Bansal, R.C., 1964. Studies in surface chemistry of carbon blacks. Part I. High temperature evacuations. *Carbon*, *1*(4), pp.451-455. doi.org/10.1016/0008-6223(64)90006-5

[27] https://www.openscad.org/ (Retrieved: 4/4/19).

[28] Vacseal, www.vacseal.com (Retrieved: 4/4/19).

[29] Heikkinen, I.T.S., Kauppinen, C., Liu, Z., Asikainen, S.M., Spoljaric, S., Seppälä, J.V., Savin, H. and Pearce, J.M., 2018. Chemical compatibility of fused filament fabrication-based 3-D printed components with solutions commonly used in semiconductor wet processing. *Additive Manufacturing*, *23*, pp.99-107. doi.org/10.1016/j.addma.2018.07.015

[30] Brunauer, S., Emmett, P.H. and Teller, E., 1938. Adsorption of gases in multimolecular layers. *Journal of the American chemical society*, *60*(2), pp.309-319. doi.org/10.1021/ja01269a023

[31] Wang, X., Zhao, L., Fuh, J.Y.H. and Lee, H.P., 2019. Effect of Porosity on Mechanical Properties of 3D Printed Polymers: Experiments and Micromechanical Modeling Based on X-Ray Computed Tomography Analysis. *Polymers*, *11*(7), p.1154. doi.org/10.3390/polym11071154

[32] Rodriguez, J.F., Thomas, J.P. and Renaud, J.E., 2000. Characterization of the mesostructure of fused-deposition acrylonitrile-butadiene-styrene materials. *Rapid Prototyping Journal*, *6*(3), pp.175-186. doi.org/10.1108/13552540010337056

[33] Bellehumeur, C., Li, L., Sun, Q. and Gu, P., 2004. Modeling of bond formation between polymer filaments in the fused deposition modeling process. *Journal of Manufacturing Processes*, *6*(2), pp.170-178. doi.org/10.1016/S1526-6125(04)70071-7

[34] Lam, C.X.F., Mo, X.M., Teoh, S.H. and Hutmacher, D.W., 2002. Scaffold development using 3D printing with a starch-based polymer. *Materials Science and Engineering: C*, *20*(1-2), pp.49-56. doi.org/10.1016/S0928-4931(02)00012-7

[35] Peltonen, P., Vuorinen, V., Marin, G., Karttunen, A.J. and Karppinen, M., 2018. Numerical study on the fluid dynamical aspects of atomic layer deposition process. *Journal of Vacuum Science & Technology A: Vacuum, Surfaces, and Films*, *36*(2), p.021516. doi.org/10.1116/1.5018475

[36] Application Notes on Vacseal, https://www.2spi.com/catalog/documents/Vacseal-App-Notes.pdf (Retrieved: 4/4/19).

[37] Vacseal SDS, http://www.vacseal.net/wp-content/uploads/2017/08/GHS-SDS-Vacseal-II-High-Vacuum-Sealant-clear-Liquid-7-15-2016.pdf (Retrieved: 4/4/19).

[38] NIST Webbook, https://webbook.nist.gov/ (Retrieved: 4/4/19).

[39] Walter, N.A. and Scialdone, J.J., 1997. Outgassing Data for Selecting Spacecraft Materials. Revision 4. NASA NTRS.

[40] NASA Outgassing Database, https://outgassing.nasa.gov/ (Retrieved: 4/4/19).

[41] Sefa, M., Ahmed, Z., Fedchak, J.A., Scherschligt, J. and Klimov, N., 2016. Gas uptake of 3D printed acrylonitrile butadiene styrene using a vacuum apparatus designed for absorption and desorption studies. *Journal of Vacuum Science & Technology A: Vacuum, Surfaces, and Films*, *34*(6), p.061603. doi.org/10.1116/1.4965304

[42] Grinham, R. and Chew, A., 2017. A Review of Outgassing and Methods for its Reduction. *Applied Science and Convergence Technology*, *26*(5), pp.95-109. doi.org/10.5757/ASCT.2017.26.5.95

[43] G.P. Beukema, Cursus Vacuumtechnologie (2016) (Retrieved: 12/12/16).

[44] Norton, F.J., 1963. Gas permeation through Lexan polycarbonate resin. *Journal of Applied Polymer Science*, *7*(5), pp.1649-1659. doi.org/10.1002/app.1963.070070507

[45] Pasanen, T.P., von Gastrow, G., Heikkinen, I.T., Vähänissi, V., Savin, H. and Pearce, J.M., 2019. Compatibility of 3-D printed devices in cleanroom environments for semiconductor

processing. *Materials Science in Semiconductor Processing*, *89*, pp.59-67. doi.org/10.1016/j.mssp.2018.08.027

[46] Sugimoto, M., Ishikawa, M. and Hatada, K., 1995. Toughness of polypropylene. *Polymer*, *36*(19), pp.3675-3682. doi.org/10.1016/0032-3861(95)93769-I

### Credit Author Statement

CRediT roles: Conceptualization:Hele Savin and Joshua M. Pearce; Data curation: Ismo T. S. Heikkinen, Giovanni Marin, Nupur Bihari, Craig Ekstrum, Pierce J. Mayville, Yuhuan Fei; Formal analysis: Ismo T. S. Heikkinen, Giovanni Marin, Nupur Bihari,Yun Hang Hu, Maarit Karppinen, Hele Savin and Joshua M. Pearce; Funding acquisition:Yun Hang Hu, Maarit Karppinen, Hele Savin and Joshua M. Pearce; Investigation: Ismo T. S. Heikkinen, Giovanni Marin, Nupur Bihari,Yun Hang Hu, Maarit Karppinen, Hele Savin and Joshua M. Pearce; Methodology:Ismo T. S. Heikkinen, Giovanni Marin, Nupur Bihari,Yun Hang Hu, Maarit Karppinen, Hele Savin and Joshua M. Pearce; Resources: Yun Hang Hu, Maarit Karppinen, Hele Savin and Joshua M. Pearce; Supervision:Yun Hang Hu, Maarit Karppinen, Hele Savin and Joshua M. Pearce; Validation:Ismo T. S. Heikkinen, Giovanni Marin, Nupur Bihari; Visualization:Ismo T. S. Heikkinen, Giovanni Marin, Nupur Bihari; Roles/Writing - original draft:Ismo T. S. Heikkinen, Giovanni Marin, Nupur Bihari, Hele Savin and Joshua M. Pearce; Writing - review & editing:Ismo T. S. Heikkinen, Giovanni Marin, Nupur Bihari Craig Ekstrum, Pierce J. Mayville, Yuhuan Fei,Yun Hang Hu, Maarit Karppinen, Hele Savin and Joshua M. Pearce.

**Declaration of competing interest**

The authors declare that they have no known competing financial interests or personal relationships that could have appeared to influence the work reported in this paper.

Highlights:

- Low cost 3D printing not used for vacuum systems
- Surface treatments on 3-D printed components to mitigate outgassing explored
- Atomic layer deposition provides barrier coating to reduce outgassing
- Vacuum compatible open-source scientific hardware is presented.